Prompt fission neutron spectra from fission induced by 1 to 8 MeV neutrons on ^{235}U and ^{239}Pu using the double time-of-flight technique

S. Noda,* R. C. Haight,† R. O. Nelson, M. Devlin, and J. M. O'Donnell
Los Alamos Neutron Science Center, Los Alamos National Laboratory, Los Alamos, New Mexico 87545, USA

A. Chatillon, T. Granier, G. Bélier, and J. Taieb
CEA, DAM, DIF, F-91297 Arpajon, France

T. Kawano and P. Talou
Theoretical Division, Los Alamos National Laboratory, Los Alamos, New Mexico 87545, USA
(Received 8 June 2010; published 10 March 2011)

Prompt fission neutron spectra from ^{235}U and ^{239}Pu were measured for incident neutron energies from 1 to 200 MeV at the Weapons Neutron Research facility (WNR) of the Los Alamos Neutron Science Center, and the experimental data were analyzed with the Los Alamos model for the incident neutron energies of 1–8 MeV. A CEA multiple-foil fission chamber containing deposits of 100 mg ^{235}U and 90 mg ^{239}Pu detected fission events. Outgoing neutrons were detected by the Fast Neutron-Induced γ-Ray Observer array of 20 liquid organic scintillators. A double time-of-flight technique was used to deduce the neutron incident energies from the spallation target and the outgoing energies from the fission chamber. These data were used for testing the Los Alamos model, and the total kinetic energy parameters were optimized to obtain a best fit to the data. The prompt fission neutron spectra were also compared with the Evaluated Nuclear Data File (ENDF/B-VII.0). We calculate average energies from both experimental and calculated fission neutron spectra.

DOI: 10.1103/PhysRevC.83.034604 PACS number(s): 25.85.Ec, 24.75.+i

I. INTRODUCTION

When a nuclear fission reaction occurs, the immediate products are usually two highly excited fission fragments, which then decay by emitting several prompt neutrons and γ rays. This deexcitation process is a compound nuclear reaction, and the prompt neutron energy spectrum can be understood as a sequential emission of neutrons from these moving fragments [1]. The Los Alamos (or Madland-Nix) model [2] has been commonly and successfully used over the years to predict the prompt fission neutron spectrum called χ, and the average number of prompt neutrons per fission $\overline{\nu}$, as functions of both the fissioning nucleus and its excitation energy. Both of these quantities are averaged over the distribution of initial fission fragments. The experimental neutron-emission data can serve as a test of the Los Alamos model, which is widely used in nuclear technology. In addition, the data provide valuable information on the fundamental understanding of the neutron induced fission process.

The Los Alamos model was originally developed with 0.53, 0.60, and 7.0 MeV incident neutron data [3–8] for ^{235}U and ^{239}Pu from monoenergetic neutron source experiments. Although the model is used for these and other actinides over a wide range of incident neutron energies, only a few experiments have been performed above 1 MeV. Boykov *et al.* [9] measured the prompt fission neutron spectra at 2.9 and 14.7 MeV for ^{235}U. Knitter *et al.* measured the fission neutron spectrum for fission induced by neutrons of 1.5, 1.9, and 2.3 MeV neutrons on ^{235}U [10] and 0.215 MeV neutrons on ^{239}Pu [11]. Staples *et al.* [12] measured prompt fission neutron spectra at 0.5, 1.5, 2.5, and 3.5 MeV for ^{235}U and ^{239}Pu. Experimental average kinetic energies are also available [13–15]. Except for some measurements made before 1970, these data constitute the experimental database for neutron-induced fission of these isotopes. There are large gaps in the experimental data, especially for ^{239}Pu but also for ^{235}U, both for incident neutron energies and for important parts of the outgoing neutron spectra (e.g., below 1 MeV and above 8 MeV). Furthermore, if the fission neutron spectrum varies slowly with incident neutron energy, as predicted by several models, some data sets are inconsistent with others. Because of these deficiencies in experimental data, evaluated data files inevitably rely on models to predict the spectra. These models rest on model parameters that are obtained by the best fits to the scarce experimental data.

The above referenced data are based on monoenergetic neutron sources, for example, those based on DD and DT reactions [9], the $P+T$ reaction [10], and the ^{7}Li(p,n) reaction [11,12]. Generally these monoenergetic neutron sources are intense, but for such neutron facilities, each incident neutron energy corresponds to a separate experiment with potential systematic effects from possible instabilities in the detectors and electronics. Another limitation of some of the previous measurements [10–12] is that thick samples of actinides were used, and only fission neutrons above the incident neutron energy were detected. Our approach is to address both of these issues with the use of a continuous ("white") source of incident neutrons and an ionization chamber to detect fissions. The white source enables measurements at all incident energies in one experiment. The ion chamber identifies fissions

*Present address: Kyushu University, 744 Motooka Nishi-ku, Fukuoka 819-0395 Japan.
†haight@lanl.gov

so that fission neutrons could be detected both below and above the source neutron energy.

The Weapons Neutron Research facility (WNR) at the Los Alamos Neutron Science Center (LANSCE) [16,17] produces a continuous-in-energy spectrum of neutrons by spallation reactions of the pulsed 800 MeV proton beam on a tungsten target. The produced neutrons induced fission reactions in a fission ionization chamber that contained samples of both ^{235}U and ^{239}Pu. Ratios of the fission neutron spectra from these two isotopes could therefore be obtained in a single experiment.

The present measurements were carried out at the Fast Neutron-Induced γ-Ray Observer (FIGARO) array [18] at WNR/LANSCE. Ethvignot *et al.* [19,20] performed a similar experiment with an earlier version of FIGARO. They reported average energies of the prompt fission neutron spectra from ^{235,238}U up to 200 MeV using fission ionization chambers that contained about 380 mg of pure ^{238}U in one chamber and 348 mg of ^{235}U in the other. In the present measurement, the fission ionization chamber contained smaller amounts of the samples, 100 mg ^{235}U and 90 mg ^{239}Pu, but the array of neutron detectors was increased in number from 6 to 20. By having both ^{235}U and ^{239}Pu in the same fission ionization chamber, information on the relative fission neutron spectra for these two isotopes could be obtained.

The fission neutron spectra of ^{235}U and ^{239}Pu were measured here for incident neutrons in the range 1–200 MeV. In this article, we report the data below 8 MeV in order to focus mainly on first-chance fission, which can be described by a relatively simple model calculation. The experimental results are compared with the evaluated data in Evaluated Nuclear Data File (ENDF/B-VII.0) [21]. Using the Los Alamos model, we fit the experimental fission neutron spectra with the total kinetic energy (TKE) parameter. We compare the average kinetic energies of the prompt neutrons that were obtained from the experiments, the ENDF/B-VII.0 data, and the Los Alamos model calculations. An extensive presentation of the experimental details and results is given in an available report [22].

II. EXPERIMENT

A. Experimental setup

The experiment was carried out using the FIGARO facility at WNR/LANSCE. The incident neutron beam at WNR is produced by the 800 MeV proton beam, bunched to 200 ps, striking a tungsten target. The produced neutrons have a spallation spectrum ranging from 0.1 to several hundred MeV. For this experiment, the energies of neutrons incident on the fission chamber were measured by the time of flight between the neutron-production target and the fission chamber over a 22.74 m flight path. To suppress low-energy neutrons, attenuators of 1.27 cm of Pb and 1.27 cm of polyethylene (CH_2) were placed in the beam about 6 m from the source. The neutron beam was collimated to 2.8 cm in diameter by a series of CH_2, Cu, and Pb inserts ending 0.83 m before the fission ionization chamber.

The multiplate fission ionization chamber [23] (pictured in Figs. 1 and 2), which was fabricated in 1968 by CEA in France, contained the target materials. The actinides ^{235}U and ^{239}Pu were deposited on 0.125 mm thick platinum backings,

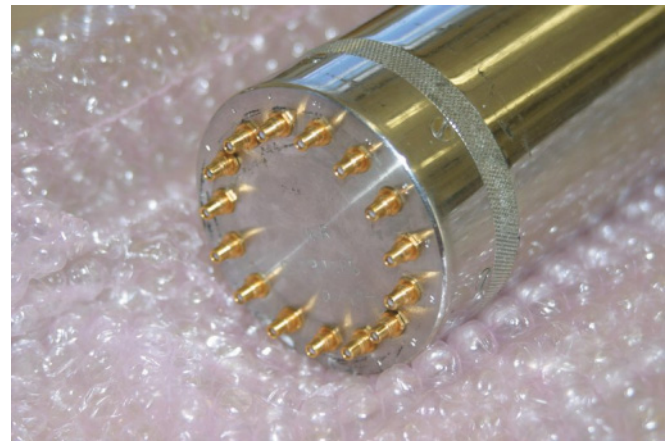

FIG. 1. (Color online) The CEA fission chamber, showing the coaxial signal feedthroughs.

which served as electrodes in the fission chamber. For ^{235}U, there were 11 such electrodes, and for ^{239}Pu, there were the same number. The electrodes for the ^{235}U foils were connected in parallel internally in the chamber. Separately, those for the ^{239}Pu foils were similarly connected. A fission signal from one or the other set of foils had four functions: It triggered the data acquisition; it indicated which actinide fissioned; it served as the stop signal for time of flight for neutrons from the production target, from which the incident energy was calculated; and it was the start signal for measuring the time of flight of fission neutrons to the neutron detector, which gave the fission neutron energy for that event.

The FIGARO array of 20 neutron detectors is used to detect the fission neutrons (see Fig. 3). These detectors are Eljen EJ301 liquid organic scintillators, 12.5 cm in diameter and 5 cm thick, each being viewed by a Hamamatsu R1250A 5 inch photomultiplier tube. The distance between the fission chamber and each neutron detector was measured accurately and was approximately 1 m for each neutron detector. The EJ301 scintillator, which is very similar to NE213 and BC501A, has different responses to neutrons and γ rays; it uses the higher linear energy transfer (LET) of recoil protons from

FIG. 2. (Color online) The CEA fission chamber, showing the overall appearance.

FIG. 3. (Color online) The FIGARO array, consisting of 20 EJ301 neutron detectors and a BaF_2 γ-ray detector.

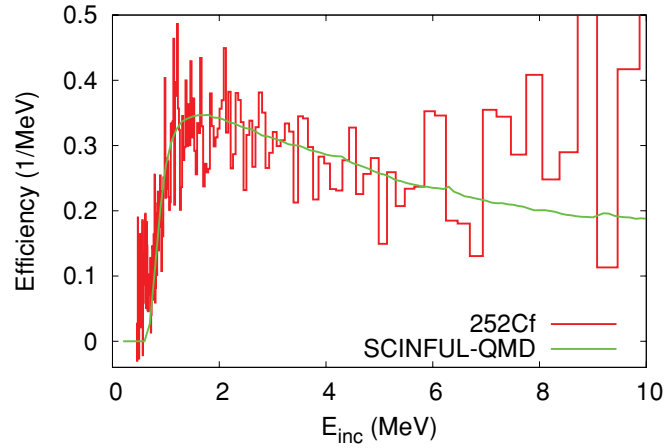

FIG. 4. (Color online) An example of efficiency of one EJ301 neutron detector. The histogram is the result of the ^{252}Cf experiment, and the dotted curve is the SCINFUL-QMD calculation. Statistical uncertainties account for fluctuations in the experimental data.

n-p interactions as opposed to lower LET from fast electrons produced by γ rays to produce signals of different shape. Neutrons incident on the scintillator were separated from γ rays by pulse-shape discrimination (PSD).

In addition to the neutron detectors, γ-ray output from fission events can be investigated with a BaF_2 scintillator. The γ-ray detector is located at 90° relative to the beam direction on the opposite side of the neutron detectors. A 5 cm thick block of CH_2 is placed in front of the scintillator to reduce the number of neutrons reaching the γ-ray detector. In this study, the γ-ray detector was used to calibrate the efficiency of the neutron detector with a ^{252}Cf source, as described below.

To determine incident and emission neutron energies, a double time-of-flight method was used. All times, those of the fission chamber and the neutron detector signals, were measured relative to the proton beam pulse at the neutron production target. Thus the fission neutron time of flight (and therefore its energy) was determined by subtracting the time-to-digital converter (TDC) output for the fission chamber from that of the neutron detector.

The foreground data analyzed for this work were taken in 338 hours of beam time at WNR/LANSCE with a typical proton beam current of 1.8 μA. In addition, background data with fake fission triggers (see below) were taken for an additional 65 hours.

B. Calibrations

The neutron detectors were originally set up with a ^{60}Co calibration source to set the discriminator thresholds at 30 keV electron equivalent energy. Because of the nonlinearity of the response to proton recoils from the n-p scattering, this 30 keV electron equivalent level corresponds to a threshold of 300 keV proton-recoil energy and a lower limit for the energy of the detected neutrons of 300 keV [24].

The efficiency of the neutron detectors was determined using a ^{252}Cf spontaneous fission neutron source placed on top of the fission chamber to give direct fission neutrons as well as the small number that are down-scattered by the chamber materials. Fission events from this source were indicated by γ rays detected by the BaF_2 scintillator. We measured the efficiencies of each neutron detector with the ^{252}Cf source, and an example is shown in Fig. 4. To model the efficiency and to reduce the statistical uncertainties, the SCINFUL-QMD code [25,26] was used. A threshold energy in the response function was searched to obtain the best agreement with the ^{252}Cf data in the energy range 0.5–1.5 MeV, where we believe the ^{252}Cf data are reliable. Above 6 MeV, the background subtraction is significant and introduces a further systematic uncertainty. However, given the best fit to the ^{252}Cf data (see, e.g., Fig. 4), we can have confidence in adopting the SCINFUL-QMD calculations for the efficiencies of the detectors.

III. ANALYSIS

The fission chamber produces signals by both fission events and α decays. First we recorded all ADC and TDC outputs which may contain the α background. A gate is set on the fission signal pulse height to start measuring the energies for both incident and outgoing neutrons. The time relative to the neutron spallation source pulse gives the energy of incident neutron, which is calculated as

$$E_n = m_n c^2 \left\{ \frac{1}{\sqrt{1-\beta^2}} - 1 \right\}, \tag{1}$$

$$\beta = \frac{l}{c\Delta_{\mathrm{ch}} \times k + l}, \tag{2}$$

where m_n is the neutron rest mass (939.565346 MeV), l is the distance between the spallation source and the fission chamber (22.74 m), Δ_{ch} is the number of channels between the γ flash from the neutron-production target and the TDC channel in the time spectra, k is the time per channel (0.5 ns/ch), and c is the speed of light (2.99792×10^8 m/s).

Because the statistics of coincident fission and fission-neutron events are low for this measurement, the contribution of background events in the time-difference spectra (difference between two time spectra) can be significant even after we apply PSD cuts. The main background source is thought to be scattered neutrons from materials of the fission chamber,

such as the platinum backings, or from backgrounds in the experiment room. These neutrons can result in accidental coincidences with the fission chamber pulses. To estimate the background, we generate a fake-fission signal with a pulser. Keeping the experimental setup as is, we do not take a signal from the fission chamber but instead put pulses (∼10 kHz) from the pulser into the electronic circuits in place of the real fission signal so that the contribution of background neutrons can be quantified. This pulser rate was much higher than the rate of real fissions, and therefore the statistics in the fake-fission runs were much better than those of real fissions. The background measurements were done with the beam on, as the background rate varies with time after the neutron source pulse. The pulser was not correlated in time with the beam pulse so that it randomly sampled the various incident neutron times of flight. The background could thereby be quantified for each incident neutron energy in one run.

In our experiments, the foreground statistics are poor, and there are some zero counts in the energy-binned foreground spectra so that it may be inappropriate to assume Gaussian distributions for the data. The error bars of foreground events are estimated with ROOFIT [27] using the Poisson distribution, which is not symmetric. Here we describe the upper side of the error bar, $\Delta N_{\mathrm{F,\,high}}$, and the lower side, $\Delta N_{\mathrm{F,\,low}}$.

The background statistics are thought to be good enough to assume the Gaussian distribution. In normalizing the fake-fission background, the uncertainties are determined at every TDC channel of the fission chamber. We assume that the statistical distributions of fake-background neutrons are Gaussian with the uncertainty ΔN_{BKG}.

In subtracting the background from the foreground, a proper treatment of the uncertainties needs to be considered. Generally, Poisson distributions cannot be treated correctly, assuming that they are Gaussian. In this analysis, we consider the asymmetric property of Poisson distributions by separating the error bars as follows:

$$\Delta N_{\mathrm{high}} = \sqrt{(\Delta N_{\mathrm{F,\,high}})^2 + (\Delta N_{\mathrm{BKG}})^2}, \tag{3}$$

$$\Delta N_{\mathrm{low}} = \sqrt{(\Delta N_{\mathrm{F,\,low}})^2 + (\Delta N_{\mathrm{BKG}})^2}, \tag{4}$$

where ΔN_{high} and ΔN_{low} are the uncertainties of upper and lower sides after error propagation. Note that $\sigma_{\mathrm{high}} + \sigma_{\mathrm{low}}$ in a Poisson distribution contains 68% confidence, which is approximately the same as $\pm 1\sigma$ in a Gaussian distribution. This is schematically shown in Fig. 5.

First the data were binned in bins 1 MeV wide of the incident neutron energy in the energy range 1–8 MeV. We converted the time-difference spectra into energy spectra, using the fission-γ peak in the time-difference spectrum as the time fiducial.

The detected counts as a function of fission neutron energy were multiplied by $1/\epsilon$, where ϵ is the neutron detector efficiency calculated with SCINFUL-QMD. The data were then binned into a common energy bin scale for each individual detector and then combined into a total fission neutron spectrum.

The data for the emitted neutrons were then rebinned in order to improve the statistical uncertainty in each bin.

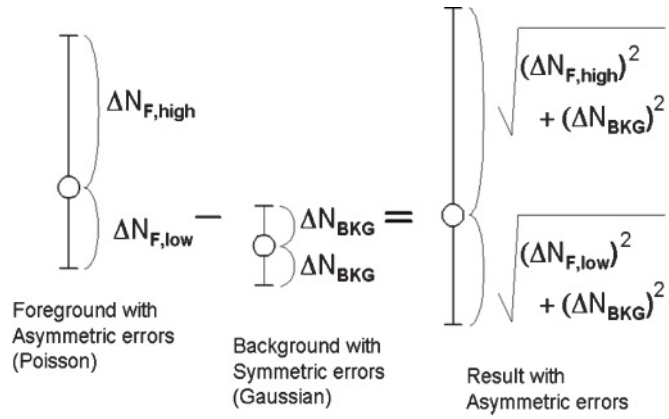

FIG. 5. Assumed error propagation.

Initially, because the experimental neutron spectra were directly converted from the time spectra channel by channel, the bins had variable widths of the outgoing neutron energy. As an example, the open circles in Fig. 6 show the ^{235}U fission spectrum for the neutron incident energy of 1–2 MeV detected by one of the EJ301 neutron detectors. Some of these bins have negative values, when the background was larger than the foreground, and although these points are not plotted on the semilogarithmic scale, they were included in the rebinned data discussed below.

Rebinning the experimental data into wider energy bins simply lowers the statistical uncertainties as $\sigma = \sqrt{\sigma_1^2 + \sigma_2^2 +, \cdots, +\sigma_n^2}/n$, where σ_i is the uncertainty on the ith bin data. To incorporate statistical fluctuations of the experimental data into the estimate of uncertainties in the averaged spectra in the wider energy bin, we calculate the chi square as

$$\frac{\chi^2}{n} = \frac{1}{n}\sum_i \frac{(N_i - \overline{N})^2}{(\Delta N_i)^2}, \tag{5}$$

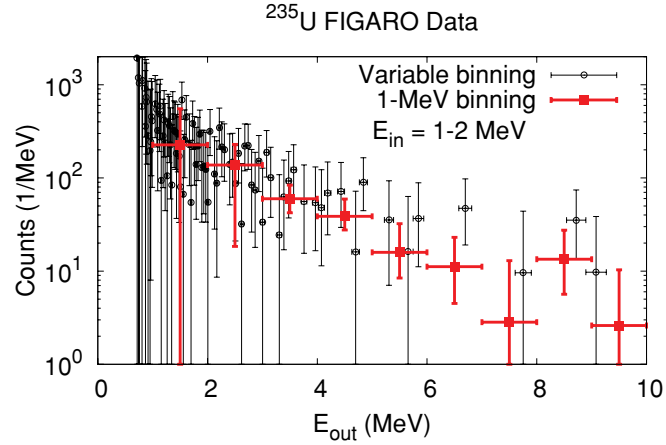

FIG. 6. (Color online) Measured ^{235}U fission neutron spectra for the neutron incident energy of 1–2 MeV. Outgoing neutron energies above 1 MeV, where neutron-γ separation is clean, are plotted. The black open circles are the data binned in variable widths of outgoing neutron energy; negative values, where the background is greater than the foreground, are not plotted. The red closed squares are the rebinned data in 1 MeV wide bins.

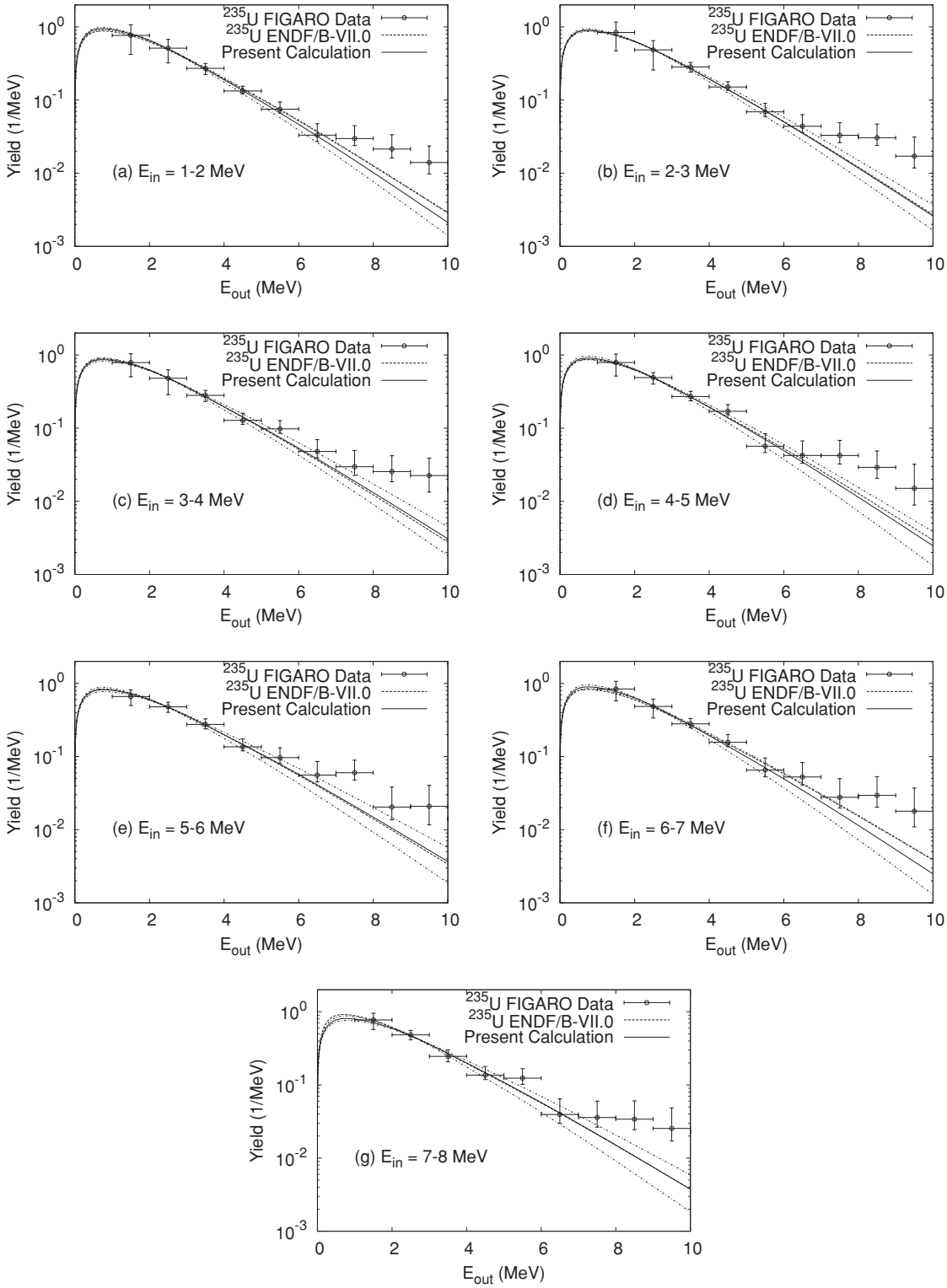

FIG. 7. ^{235}U fission neutron spectra averaged over 1 MeV incident energy intervals. The dashed curves are the Los Alamos model calculations in ENDF/B-VII.0. The solid curves are the application of this model fitted to the present experimental data, and a $\pm 1\sigma$ error band in the calculations is indicated by the dotted curves. The spectra are normalized to unity by integrating the spectra in the 2.0–6.5 MeV emission energy range.

where the index i is for the measured data before rebinning, n is the number of smaller bins in the wider bin, N_i is a number of counts, $\overline{N}$ is an average count in the measurement, and ΔN_i is given by Eqs. (3) and (4). We calculate the chi square values for each 1 MeV bin, and when $\sqrt{\chi^2/n} > 1$, we multiply the error bars by $\sqrt{\chi^2/n}$. Chi squares are calculated

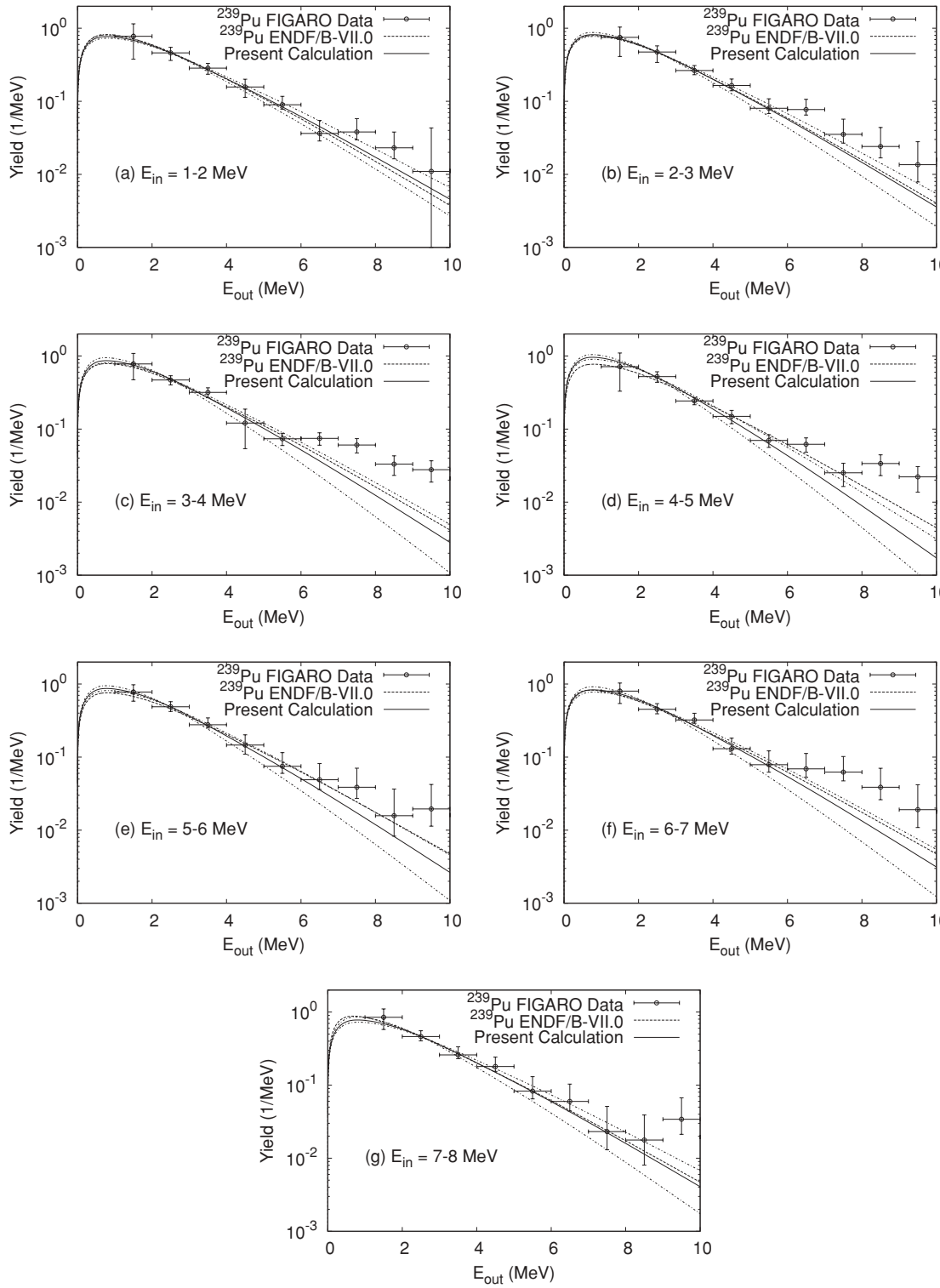

FIG. 8. ^{239}Pu fission neutron spectra averaged over 1 MeV incident energy intervals. The dashed curves are the Los Alamos model calculations in ENDF/B-VII.0. The solid curves are the application of this model fitted to the present experimental data, and a $\pm 1\sigma$ error band in the calculations is indicated by the dotted curves. The spectra are normalized to unity by integrating the spectra in the 2.0–6.5 MeV emission energy range.

for the upper and lower error bars. Figure 6 compares the original 100 keV binned data with the 1 MeV rebinned data.

Systematic uncertainties in the data include uncertainties in the detector efficiencies, in separation of neutrons and γ rays by PSD, and in the background subtraction. The detector

efficiencies are believed to be accurate to about 5% in the relative efficiency as a function of neutron energy. Near the threshold for neutron detection, this uncertainty is somewhat higher, but we believe that for the data reported here for emitted neutron energies above 1 MeV, the 5% uncertainty is appropriate. The neutron-γ discrimination is quite clean for these neutron energies, and so we believe that the systematic uncertainty in defining the neutron and γ regions in the PSD is small.

Scattering of the fission neutrons from components of the fission chamber has been analyzed by Monte Carlo calculations [28]. The measurement is predicted to be 6% lower than the unscattered spectrum at 5 MeV and 7% lower at 8 MeV relative to the yield at 2 MeV. This correction has not been made in the data presented here. It is smaller than the uncertainties in the data in the 5–10 MeV range of emitted neutron energies. Because the effects are basically the same for ^{235}U and ^{239}Pu, there is no correction to be made to the ratio data. Any additional systematic uncertainty we believe is small in comparison to the statistical uncertainties.

Because this is not an absolute measurement but rather a measurement of the shape of the fission neutron spectra, we normalized the obtained spectra to compare with other experimental data and with theoretical calculations. The normalization was performed by integrating the experimental data in the 2.0–6.5 MeV emission energy range and setting this integral to unity. The theoretical model calculations are also normalized in the same energy range for comparisons.

IV. RESULTS AND DISCUSSION

The experimental results for ^{235}U and ^{239}Pu are shown in Figs. 7 and 8. The dashed lines are the evaluated fission spectra in ENDF/B-VII.0 [21], and the solid lines are our Los Alamos model calculation results, which we discuss below. All the experimental results, the ENDF/B-VII.0 evaluated data, and our model calculation results are normalized to unity by integrating the values in the 2.0–6.5 MeV emission energy range. Although the experimental data have rather large uncertainties, the agreement of the ENDF/B-VII.0 evaluations and our experimental data is fair in general. Especially for the 1–2 MeV neutron incident data, the Los Alamos model calculation reproduces our data well up to 6 MeV outgoing neutron energy for both ^{235}U and ^{239}Pu cases.

For many of the spectra, there seem to be excess fission neutrons above 8 MeV. The predicted spectra drop off at these higher emission energies, down from the peak near 1 MeV by a factor of 15 at 6 MeV and a factor of 60 at 8 MeV, for example, and backgrounds are more important for these higher neutron energies. It is therefore difficult to argue for the existence of an excess of high-energy fission neutrons from the present data.

The fission neutron spectrum in ENDF/B-VII.0 is calculated with the Los Alamos model [2] as

$$\chi(E_{\rm out}) = \frac{1}{2\sqrt{E_f}T_m^2}\int_{(\sqrt{E_{\rm out}}-\sqrt{E_f})^2}^{(\sqrt{E_{\rm out}}+\sqrt{E_f})^2}\sigma_R(\epsilon)\sqrt{\epsilon}d\epsilon \times \int_0^{T_m} k(T)T\exp(-\epsilon/T)dT, \quad (6)$$

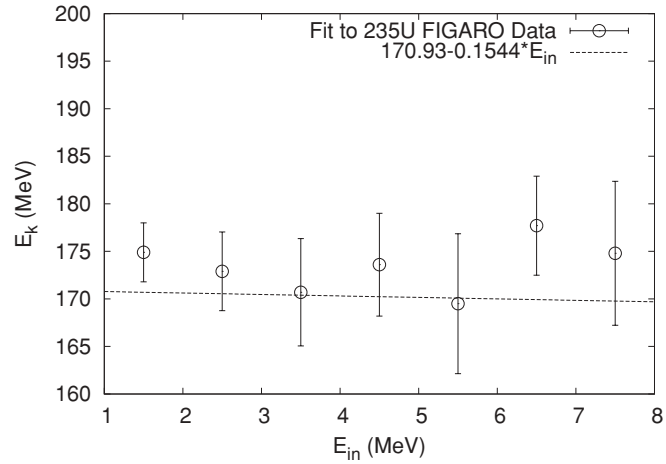

FIG. 9. Estimated total kinetic energies E_k for ^{235}U. The dashed line represents the systematics obtained by Madland [30].

where E_f and T_m are the average kinetic energy and the maximum nuclear temperature of the fission fragments, $k(T)$ the temperature-dependent normalization integral, and $\sigma_R(\epsilon)$ is the inverse reaction cross section calculated with the optical model. The maximum temperature T_m can be related to the neutron binding energy B_n, the incident energy $E_{\rm in}$, the total energy release E_r, and the total kinetic energy E_k as $aT_m^2 = E_r + B_n + E_{\rm in} - E_k$, where a is the level density parameter of the compound nucleus. Starting from the same model parameter values as used in the ENDF/B-VII.0 evaluations, we adjusted the total kinetic energy E_k to obtain the best fit to our experimental data because $\chi(E_{\rm out})$ is most sensitive to E_k and E_r. The parameter fitting was performed with the Bayesian model parameter estimation code KALMAN [29].

The estimated E_k values for ^{235}U and ^{239}Pu are shown in Figs. 9 and 10 as a function of the neutron incident energy. The estimated uncertainties on E_k are typically 2%–4%, which are somewhat larger than experimental data in the literature. Madland [30] estimated the energy dependence of E_k from experimental data available and obtained simple linear

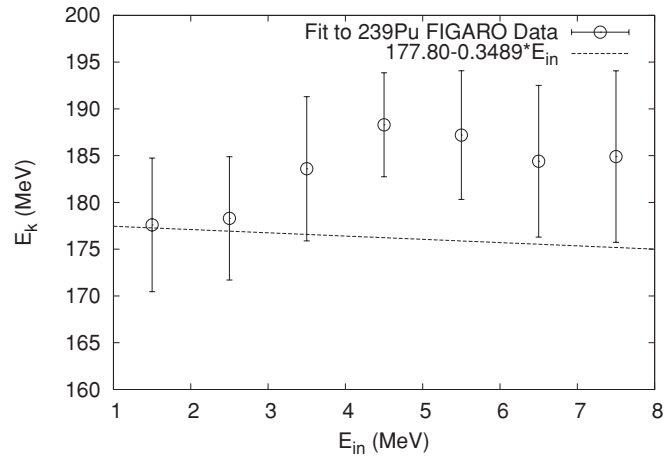

FIG. 10. Estimated total kinetic energies E_k for ^{239}Pu. The dashed line is the systematics obtained by Madland [30].

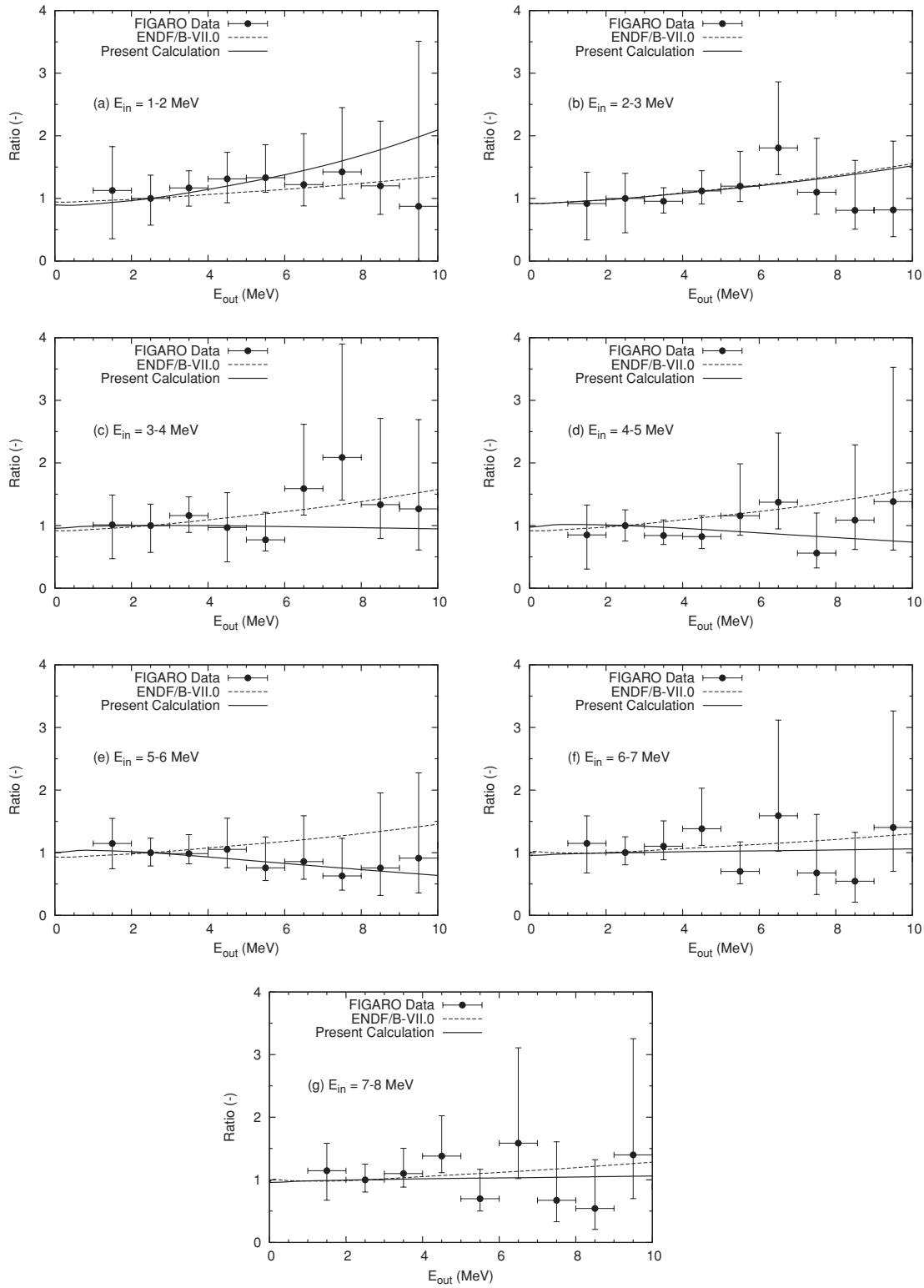

FIG. 11. Ratios of fission neutron spectra of ^{239}Pu to ^{235}U, normalized to unity in the 2–3 MeV outgoing energy range.

functional forms as

$$E_k = 170.93 - 0.1544E_{\rm in} \quad \text{MeV} \tag{7}$$

for ^{235}U and

$$E_k = 177.80 - 0.3489E_{\rm in} \quad \text{MeV} \tag{8}$$

for ^{239}Pu, where the incident energy $E_{\rm in}$ is in mega electron volts. These systematics are also shown in Figs. 9 and 10 by the dashed lines. Comparing our derived E_k values with the systematics by Madland, relatively small deviations are seen in the case of ^{235}U. However, the difference reaches

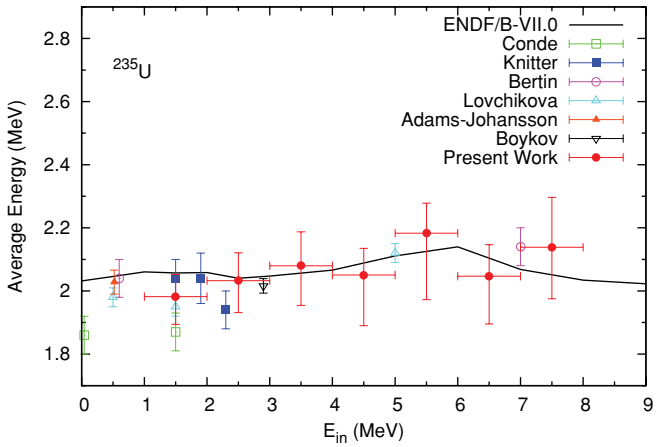

FIG. 12. (Color online) Average energies of ^{235}U fission spectra calculated from fits to the present data (present work) for the full range of emitted neutron energies compared with values from the ENDF/B-VII.0 evaluation. Literature values are from Knitter *et al.* [10], Condé and During [15], Bertin *et al.* [4,5], Lovchikova and Trufanov [13], Adams, Johansson, and their colleagues [3,7,8], and Boykov *et al.* [9]. Data points near 0.5 and 1.5 MeV have been slightly displaced from each other horizontally for clarity.

7% for the ^{239}Pu case. Although our data in Figs. 10 and 11 suggest TKE is energy dependent, as in Eqs. (7) and (8), the least squares analysis to the data gives different slopes with respect to incident neutron energy, especially for the ^{239}Pu case, which becomes $+1.60E_{\rm in}$ with an uncertainty of $\pm 0.71E_{\rm in}$. This inconsistency could be solved by combining more experimental and theoretical information. We emphasize that the TKE parameter was the only one adjusted in this work.

The calculated spectra with the obtained E_k values are shown in Figs. 7 and 8 by the solid lines. The KALMAN code also gives uncertainties on E_k. Putting $E_k \pm \delta E_k$ into Eq. (6), one can estimate the uncertainty bands of the calculated spectra, which are also depicted in these figures.

It is interesting to compare the fission neutron spectrum shape for ^{235}U and ^{239}Pu because the emitted neutrons from ^{239}Pu(n,f) could be more energetic than those from ^{235}U(n,f) due to the larger Coulomb energy in the system. We calculated the ratios of the ^{239}Pu fission spectrum to those from ^{235}U for both the experimental data and the Los Alamos model calculations, which are shown in Fig. 11. Because our experimental data are relative measurements, the absolute scale of the ratio data is arbitrary. We renormalized the ratio data to unity in the energy range 2–3 MeV for comparison purposes. The model calculations were also renormalized in the same way. For the ENDF/B-VII.0 evaluations, the ratios increase monotonically with the neutron outgoing energy. Our experimental data suggest that the increase is small. We also observe the opposite tendency, such as in the $E_{\rm in} =$ 5–6 MeV case. We need more precise data with higher statistics to investigate how the shapes of prompt fission neutron spectra vary with energy and with fissioning systems. Such data should have significant information to improve the Los Alamos model because the model itself does not have much freedom to change the shape of spectra.

Once the E_k values were derived from our experimental data in the energy range of 2.0–6.5 MeV, the Los Alamos model was extended below 2 MeV and above 6.5 MeV to obtain the average energy of the fission spectrum as

$$\langle E \rangle = \frac{\int \chi(E)\, E\, dE}{\int \chi(E)\, dE}. \tag{9}$$

Ethvignot *et al.* [19,20] obtained the averaged energies by fitting the experimental spectra with Maxwellian functions and then calculated the averaged energy from the fit. In this study, we employed the Los Alamos model to extrapolate the spectra for the entire outgoing energy region to obtain the average energies, which are shown in Figs. 12 and 13. The deduced average energies agree well with ENDF/B-VII.0 evaluations. In the evaluated data, the average energy drops slightly above 5 MeV, which is expected from the opening of the second-chance fission channel. Our data neither confirm nor deny this prediction due to the size of the experimental uncertainties. A more quantitative result requires higher statistics in measuring prompt fission neutrons. Nevertheless, the present experimental data do support the Los Alamos model calculations in ENDF/B-VII.0, at least within the assigned uncertainties.

New measurements ^{239}Pu prompt fission neutron spectra have recently been performed by Chatillon *et al.* [31] at the facility described here but with an improved fission chamber and improved statistics. Although their experimental data are still preliminary, further reduction in uncertainties in the

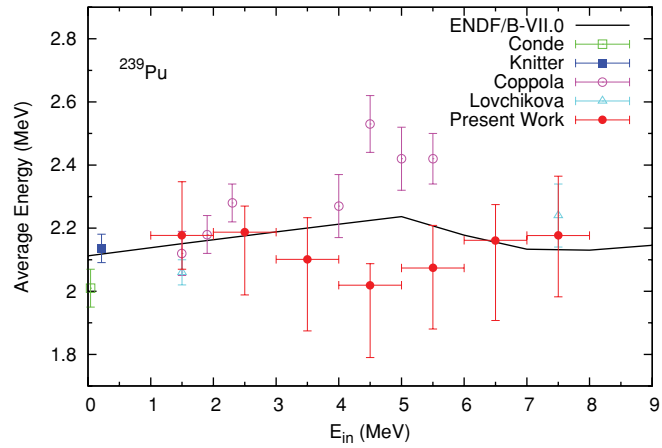

FIG. 13. (Color online) Average energies of ^{239}Pu fission spectra calculated from fits to the present data (present work) for the full range of emitted neutron energies compared with values from the ENDF/B-VII.0 evaluation. Literature values are from Knitter *et al.* [10], Condé and During [15], Coppola and Knitter [14], and Lovchikova and Trufanov [13]. Data points near 1.5 MeV have been slightly displaced from each other horizontally for clarity.

Los Alamos model calculations appear to be possible in the near future.

V. CONCLUSION

The prompt fission neutron spectra from ^{235}U and ^{239}Pu were measured for incident neutron energies from 1 to 200 MeV at WNR/LANSCE with the FIGARO array, and the experimental data were analyzed with the Los Alamos model in the incident neutron energy range of 1–8 MeV. We applied a so-called fake-background technique to estimate the background carefully. In addition, the data analysis required asymmetric probability distributions due to the Poisson nature of low counting rates. We performed the Los Alamos model calculations and adjusted the model parameters to fit the experimental data to deduce average energies of the spectra. The obtained average energies are in good agreement with the prompt fission neutron spectra in ENDF/B-VII.0 within our estimated uncertainties.

ACKNOWLEDGMENTS

One of the authors (S.N.) would like to thank Kyushu Industrial Technology Center for supporting his stay at Los Alamos to perform this work and S. A. Wender and J. Carlson for accepting him to be a visiting graduate school student in Los Alamos National Laboratory. He also thanks K. Ishibashi and N. Shigyo of Kyushu University for valuable discussions. We thank D. G. Madland for providing the Los Alamos model input parameters. This work was carried out in part under the agreement between the US Department of Energy and the French Commissariat à l'Énergie Atomique on fundamental science supporting stockpile stewardship. The experimental measurements benefited from the use of the LANSCE accelerator facility. The work at Los Alamos was carried out under the auspices of the US Department of Energy at Los Alamos National Laboratory by the Los Alamos National Security LLC under Contract No. DE-AC52-06NA25396.

[1] S. Lemaire, P. Talou, T. Kawano, M. B. Chadwick, and D. G. Madland, Phys. Rev. C **72**, 024601 (2005).
[2] D. G. Madland and J. R. Nix, Nucl. Sci. Eng. **81**, 213 (1982).
[3] P. I. Johansson and B. Holmqvist, Nucl. Sci. Eng. **62**, 695 (1977).
[4] A. Bertin, R. Bois, and J. Fréhaut, Commissariat à l'Énergie Atomique, Centre d'Études de Bruyères-le-Châtel Report No. CEA-R-4913, 1978 (unpublished).
[5] A. Bertin, R. Bois, and J. Fréhaut, Trans. Am. Nucl. Soc. **22**, 667 (1975).
[6] J. Fréhaut, A. Bertin, and R. Bois, Trans. Am. Nucl. Soc. **32**, 732 (1979).
[7] P. I. Johansson, B. Holmqvist, T. Wiedling, and L. Jeki, US National Bureau of Standards Special Publication No. 425, 1975 (unpublished).
[8] J. M. Adams, UK Atomic Energy Authority Report No. AERE-R-8636, 1977 (unpublished).
[9] G. S. Boykov, V. D. Dmitriev, G. A. Kudyaev, Y. B. Ostapenko, M. I. Svirin, and G. N. Smirenkin, Yad. Fiz. **53**, 628 (1991).
[10] H.-H. Knitter, M. M. Islam, and M. Coppola, Z. Phys. **257**, 108 (1972).
[11] H.-H. Knitter, Atomkernergie **26**, 76 (1975).
[12] P. Staples, J. J. Egan, G. H. R. Kegel, A. Mittler, and M. L. Woodring, Nucl. Phys. A **591**, 41 (1995).
[13] G. N. Lovchikova and A. M. Trufanov, Vop. At. Nauki Tekhn. Ser. Yadernye Konstanty **1996**, 102 (1996).
[14] M. Coppola and H.-H. Knitter, Z. Phys. **232**, 286 (1970).
[15] H. Condé and G. During, Ark. Fys. **29**, 313 (1965).
[16] P. W. Lisowski, C. D. Bowman, G. J. Russell, and S. A. Wender, Nucl. Sci. Eng. **106**, 208 (1990).
[17] P. W. Lisowski and K. F. Schoenberg, Nucl. Instrum. Methods A **562**, 910 (2006).
[18] D. Rochman, R. C. Haight, J. M. O'Donnell, M. Devlin, T. Ethvignot, and T. Granier, Nucl. Instrum. Methods A **523**, 102 (2004).
[19] T. Ethvignot, M. Devlin, R. Drosg, T. Granier, R. C. Haight, B. Morillon, R. O. Nelson, J. M. O'Donnell, and D. Rochman, Phys. Lett. B **575**, 221 (2003).
[20] T. Ethvignot, M. Devlin, M. Duarte, T. Granier, R. C. Haight, B. Morillon, R. O. Nelson, J. M. O'Donnell, and D. Rochman, Phys. Rev. Lett. **94**, 052701 (2005).
[21] M. B. Chadwick *et al.*, Nucl. Data Sheets **107**, 2931 (2006).
[22] R. C. Haight, S. Noda, and J. M. O'Donnell, LANSCE-NS Progress Report No. LA-UR-08-2585, 2008 (unpublished).
[23] M. Soleilhac, J. Fréhaut, and J. Gauriau, J. Nucl. Energy **23**, 257 (1969).
[24] K. H. Maier and J. Nitschke, Nucl. Instrum. Methods **59**, 227 (1968).
[25] J. K. Dickens, Oak Ridge National Laboratory Report No. ORNL-6462, 1988 (unpublished).
[26] D. Satoh, T. Sato, N. Shigyo, and K. Ishibashi, Japan Atomic Energy Agency JAEA-Data/Code No. 2006-023, 2006 (unpublished).
[27] [http://roofit.sourceforge.net/docs/RooFit_Users_Manual_2.07-29.pdf].
[28] T. Taddeucci (private communication).
[29] T. Kawano and K. Shibata, Japan Atomic Energy Research Institute JAERI-Data/Code No. 97-037, 1997 (unpublished).
[30] D. G. Madland, Nucl. Phys. A **772**, 113 (2006).
[31] A. Chatillon, G. Bélier, T. Granier, B. Laurent, J. Taïeb, S. Noda, R. C. Haight, M. Devlin, R. O. Nelson, and J. M. O'Donnell, in *Proc. of the 12th International Conference on Nuclear Reaction Mechanisms, Varenna, Italy, 15–19 June 2009*, edited by F. Cerutti and A. Ferrari, CERN-Proceedings-2010-001, 239 (2010) [http://cdsweb.cern.ch/record/1233497].